

MICROCOPY RESOLUTION TEST CHART  
NATIONAL BUREAU OF STANDARDS-1963-A

12

AD-A163 290

DTIC  
ELECTE  
JAN 23 1986  
S D  
D

APPENDIX 6.

Shi, N. C. and Wright, L. D., in press. Standing waves on a pronounced bar-trough beach, Jour. Geophys. Res. (31 pp.).

DTIC FILE COPY

86 1 22 213

Unclassified

SECURITY CLASSIFICATION OF THIS PAGE (When Data Entered)

REPORT DOCUMENTATION PAGE		READ INSTRUCTIONS BEFORE COMPLETING FORM
1. REPORT NUMBER	2. GOVT ACCESSION NO.	3. RECIPIENT'S CATALOG NUMBER
	AD-A163	290
4. TITLE (and Subtitle)	5. TYPE OF REPORT & PERIOD COVERED	
Standing Waves on a Pronounced Bar Trough Beach	Technical Report 15 Feb. 1983 - 31 Dec. 1985	
	6. PERFORMING ORG. REPORT NUMBER	
7. AUTHOR(s)	8. CONTRACT OR GRANT NUMBER(s)	
N. C. Shi and L. D. Wright	Contract N00014-83-K-0198	
9. PERFORMING ORGANIZATION NAME AND ADDRESS	10. PROGRAM ELEMENT, PROJECT, TASK AREA & WORK UNIT NUMBERS	
Virginia Institute of Marine Science School of Marine Science, College of William & Mary Gloucester Point, Virginia 23062	NR 388-189	
11. CONTROLLING OFFICE NAME AND ADDRESS	12. REPORT DATE	13. NUMBER OF PAGES
Office of Naval Research Coastal Sciences Program, Code 422CS Arlington Virginia, 22217	31 December 1985	31
14. MONITORING AGENCY NAME & ADDRESS (if different from Controlling Office)	15. SECURITY CLASS. (of this report)	15a. DECLASSIFICATION/DOWNGRADING SCHEDULE
	Unclassified	
16. DISTRIBUTION STATEMENT (of this Report)		
Distribution of this document is unlimited		
17. DISTRIBUTION STATEMENT (of the abstract entered in Block 20, if different from Report)		
18. SUPPLEMENTARY NOTES		
19. KEY WORDS (Continue on reverse side if necessary and identify by block number)		
Beaches; surf zones; standing waves; edge waves; bars; numerical model; spectra.		
20. ABSTRACT (Continue on reverse side if necessary and identify by block number)		
The hypothesis that a pronounced bar-trough surf zone topography favors resonance of standing waves with antinodes located over the bar is examined. Numerical and field investigations of standing waves in a bar-trough surf zone suggest a selective trapping of wave energy at specific resonant frequencies in the subharmonic and the high frequency infragravity bands and a possible suppression of lower frequencies. The resonant frequencies predicted by the numerical model remain fairly constant throughout the tidal		

DD FORM 1 JAN 73 1473

EDITION OF 1 NOV 65 IS OBSOLETE  
S/N 0102-LF-014-4601

Unclassified

SECURITY CLASSIFICATION OF THIS PAGE (When Data Entered)

Unclassified

SECURITY CLASSIFICATION OF THIS PAGE (When Data Entered)

cycle due to the small tidal range typically associated with a bar-trough beach. Cross-shore bar migration changes the resonant frequencies. Numerical simulations show that an onshore bar migration is accompanied by a reduction in the period of the resonant wave and a decrease in the longshore wavelength of the possible edge wave mode.

S N 0102-LF-014-6601

Unclassified

SECURITY CLASSIFICATION OF THIS PAGE (When Data Entered)

STANDING WAVES ON A PRONOUNCED BAR-TROUGH BEACH

Nungjane C. Shi  
and  
L.D. Wright



Accession For	
NTIS CRA&I	<input checked="" type="checkbox"/>
DTIC TAB	<input type="checkbox"/>
Unannounced	<input type="checkbox"/>
Justification	
By	
Distribution /	
Availability Codes	
Dist	Avail and/or Special
A-1	

Virginia Institute of Marine Science, School of Marine Science, College of William and Mary, Gloucester Point, VA 23062 (U.S.A.)

## ABSTRACT

The hypothesis that a pronounced bar-trough surf zone topography favors resonance of standing waves with antinodes located over the bar is examined. Numerical and field investigations of standing waves in a bar-trough surf zone suggest a selective trapping of wave energy at specific resonant frequencies in the subharmonic and the high frequency infragravity bands and a possible suppression of lower frequencies. The resonant frequencies predicted by the numerical model remain fairly constant throughout the tidal cycle due to the small tidal range typically associated with a bar-trough beach. Cross-shore bar migration changes the resonant frequencies. Numerical simulations show that an onshore bar migration is accompanied by a reduction in the period of the resonant wave and a decrease in the longshore wavelength of the possible edge wave mode.

## INTRODUCTION

A pronounced bar-trough beach is characterized by a shallow bar with a steep shoreward face, a deep trough and a steep beach face. The steep beach face favors reflection of incoming waves and results in strong standing wave motion in the trough (Wright et al., 1986). Morphodynamically, such beaches are intermediate between the fully dissipative beaches and the highly reflective beaches (Wright and Short, 1984). On beaches subjected to large variations in the incoming wave energy, a bar-trough beach can develop from a preceding dissipative beach state. In many cases, accentuated bar-trough morphology may persist virtually year round with the bar undergoing appreciable and rapid crossshore migration (Sallenger et al., 1985; Wright et al., 1986). Unlike the more subtle bars which often surmount dissipative surf zone profiles during high energy or storm conditions, pronounced bar-trough forms prevail under more moderate energy regimes and the morphology plays a more apparent role in controlling surf zone hydrodynamics.

As in other types of surf zones, infragravity energy is important in bar-trough surf zones. It exists there as standing surf zone oscillations which may be either leaky mode standing waves or trapped mode edge waves. In either case, the standing waves may interact resonantly with the pronounced bar-trough morphology. In order for the resonant standing oscillations to be in equilibrium with the morphology, they should have their antinodes (positions of amplitude maxima of sea surface elevation) over the bar and nodes in the trough (Katoh, 1984; Symonds and Bowen, 1984). At a moderate wave energy level, a pronounced bar-trough morphology may contribute to its self-maintenance by favoring resonance at specific frequencies. Previous field observations (e.g. Wright, 1982) showed that infragravity energy in bar-trough surf zones is relatively low and is

centered at higher frequencies than in a fully dissipative surf zone. However, elucidation of the relationships of the infragravity standing waves to topography has relied mainly on speculation.

In this paper, we investigate the influences of accentuated bar-trough topography on the infragravity standing wave oscillations in the surf zone. We approach this by applying a numerical model to predict standing wave behavior over an observed bar-trough topography and comparing the results to a limited set of field observations. Of central importance in our numerical study are the positions of nodes and antinodes in the surf zone, or equivalently, the periods of standing waves that produce a node or antinode at specific locations in the surf zone. The simple expression,

$$T = \frac{2}{m} \int_0^x \frac{dx'}{gh} \quad (1)$$

where  $m=n-1/2$  for the nodal period, and  $m=n$  for the anti-nodal period,  $n$  is an integer,  $x$  is the distance from the beach face,  $g$  is gravity and  $h$  is water depth, has been used by some (eg. Gerritsen and Heteren, 1984) to estimate the node and antinode periods of leaky mode standing waves. However, equation 1 gives gross errors when applied to a sloping beach. For example, for a beach with constant slope,  $\tan \beta$ , equation 1 gives,

$$\Gamma = \frac{2}{m}, \quad \text{where} \quad \Gamma = \frac{T}{2 \sqrt{x/g \tan \beta}}. \quad (2)$$

Thus the first two nodal periods would occur at  $\Gamma=4$  and 1.33, and the first two antinodal periods would occur at  $\Gamma=2$  and 1. These estimates differ significantly from those obtained using the leaky mode solution (equation 7a) which give  $\Gamma=2.62$  and 1.14 for the first two nodes and  $\Gamma=1.64$  and 0.89 for the first two antinodes. The difference originates from the implicit assumption made in deriving equation 1 that the wave travels with speed  $\sqrt{gh}$ . This assumption fails whenever the water depth varies significantly over one wave length as is the case over beach of constant slope. For a complex

beach profile, equation 1 is far from adequate. Proper numerical models are required to deal with standing waves over a complex natural beach profile.

We introduce a numerical technique for solving for the amplitude function of a standing wave oscillation in the surf zone. Numerical predictions of the standing wave oscillations and a set of field observations are examined to study (1) the characteristics of the standing waves in a pronounced bar trough surf zone, and (2) the effects of tidal elevation changes and cross shore bar migration on the standing wave characteristics. A quantity, the total energy density of a standing wave, is defined to aid the interpretation of the field observations.

#### THEORY AND NUMERICAL TECHNIQUE

The equation governing the standing wave oscillation in the nearshore zone expressed in terms of the velocity potential  $\phi$  has the form

$$\phi_{tt} - g \nabla_H \cdot (h \nabla_H \phi) = 0. \quad (3)$$

where  $\nabla_H = (\partial/\partial x, \partial/\partial y)$ ,  $g$  is the gravitational acceleration,  $u = (u, v) = \nabla_H \phi$  is the horizontal velocity vector, and  $h$  is the water depth. The sea surface elevation,  $\eta = -\phi_t/g$ . We assume the  $x$ -axis to be shore-normal with  $x=0$  at the beach face and the  $y$ -axis to be shore-parallel.

There are two possible modes of standing waves in the nearshore zone. The leaky mode waves are the normally incident standing waves with fluid motion normal to shore and uniform alongshore. The edge wave modes are waves trapped nearshore by depth refraction and are periodic alongshore with both shore normal and shore parallel velocity components. A fundamental expression representing the sea surface elevation of the two modes is

$$\eta = a_0 \zeta(x) \cos(ky + \omega t), \quad (4)$$

with a corresponding velocity potential,

$$\phi = -(a_0 g / \omega) \zeta(x) \sin(ky + \omega t) \quad (5)$$

where  $a_0$  is the wave amplitude at  $x=0$ ,  $\zeta(x)$  is a dimensionless function expressing the offshore variation of the wave amplitude,  $k$  is the longshore wavenumber and  $\omega$  is the wave frequency. The normally-incident leaky mode wave has no longshore variation and its wavenumber vanishes.

Substituting equation 5 into equation 3 and using a length scale,  $\ell = g/\omega^2$ , we obtain a dimensionless equation,

$$(h_* \zeta')' - (k_*^2 h_* - 1) \zeta = 0, \quad (6)$$

where the prime denotes the derivative with respect to  $x_*$ ,  $x_* = x/\ell$ ,  $h_* = h/\ell$ , and  $k_* = k\ell$ . Since  $\zeta(0)=1$ , the equation can be evaluated at  $x_*=0$  to provide a second boundary condition,  $\zeta' = -1/\tan\beta_0$  at  $x_*=0$ , where  $\tan\beta_0$  is the beach slope at  $x_*=0$ . For the edge wave modes, the requirement that  $\zeta$  and  $\zeta'$  remain finite as  $x_* \rightarrow \infty$  results in the dispersion relation which expresses the relationship between edge wave frequency and wavenumber.

For a linear beach profile with constant slope  $\tan\beta$ , the leaky mode solution for equation 6 is (Eckart, 1951)

$$\zeta = J_0(2\sqrt{x_* \tan\beta}), \quad (7a)$$

and the edge wave mode solution is,

$$\zeta = \exp(-k_* x_*) L_n(2k_* x_*), \quad (7b)$$

where  $J_0$  is the zero-th order Bessel function and  $L_n$  is the LaGuerre Polynomial of order  $n$ . The dispersion relation for the edge wave modes is given by

$$\omega^2 = gk(2n+1)\tan\beta, \quad n = 0, 1, 2, \dots, \quad (8)$$

where  $n$  is the mode number and represents the number of zero-crossings (nodes) of the amplitude function.

For a beach with the exponential profile,  $h=h_0[1-\exp(-\alpha x)]$ , the amplitude function can be written in terms of a hypergeometric series of exponential functions with a dispersion relation (Ball, 1967),

$$\omega^2 = (gh_0\alpha^2/2)[(2n+1)\sqrt{1+4k^2/\alpha^2} - (2n^2+2n+1)] \quad (9)$$

provided

$$n(n+1) \leq \omega^2/(\alpha^2 gh_0). \quad (10)$$

For complex beach profiles such as those of bar-trough type beaches, equation 6 can be solved using a numerical technique. By defining  $X_1=\zeta$ , and  $X_2=\zeta'$ , we can convert equation 6 into two first order ordinary differential equations,

$$X_1' = X_2, \text{ and } X_2' = [(k_*^2 h_* - 1)X_1 - h_* X_2]/h_* \quad (11a, 11b)$$

The boundary conditions become  $X_1(0)=1$ , and  $X_2(0)=-1/\tan\beta_0$ , and that both  $X_1$  and  $X_2$  remain finite as  $x_* \rightarrow \infty$ . Given a beach profile and a standing wave frequency, the two differential equations can be numerically integrated to find the amplitude function.

We developed a numerical algorithm for solving equations 11a and 11b for the leaky and the edge wave modes. The discussion that follows is based on the edge wave solution. To obtain the leaky mode solutions, one simply sets the wavenumber to zero. The algorithm is based on the observations that: (1) the wavenumbers of all of the allowable edge wave modes have an upper bound, and (2) the number of the zero-crossings of the amplitude function and its derivative increase with decreasing wavenumber and cannot be greater than the mode number. The subroutine DVERK of the International Mathematical and Statistical Library (IMSL) developed from the Runge-Kutta-Verner fifth and sixth order method (Hull et al., 1976) is used to carried out the integration.

The upper bound of all the wavenumbers is the wavenumber of the mode-zero edge wave. As the mode number increases, the wavenumber decreases, and

vice versa. The algorithm relies on a check of the numbers of the zero crossings of  $X_1$  and  $X_2$ , which correspond respectively to the nodes and antinodes (for  $\zeta$ ) of the standing wave. Initially, the dispersion relation for the constant slope beach (equation 8) is used to estimate an upper bound,  $k_{*up}$ , of the wavenumber and  $k_{*low}=0$  is used as lower bound. Numerical integration along increasing  $x_*$  is carried out with DVERK using an initial trial wavenumber,  $k_{*0}=(k_{*up}+k_{*low})/2$ . The number of zero-crossings,  $n_N$  for the nodes is identified at each step of the integration. Through numerous tests, we found that once  $X_1$  exceeds a value on the order of 10, continuing integration along increasing  $x_*$  then sharply increases  $|X_1|$  monotonically. Thus, if  $n_N > n$ , where  $n$  is the desired mode number, before  $X_1$  becomes greater than 0(10), then the wavenumber used is too small and a new wavenumber,  $(k_{*0}+k_{*up})/2$  is used to repeat the integration. This time, the original trial  $k_{*0}$  becomes the lower bound of the wavenumber,  $k_{*low}$ . On the other hand, if  $n_N < n$ , a new wavenumber,  $(k_{*0}+k_{*low})/2$ , is used to repeat the integration and the original  $k_{*0}$  becomes the new upper bound of the wavenumber. The procedure is repeated until an error index, defined as  $e_r=(k_{*}(new)/k_{*}(old) - 1)$  is within a desired accuracy. The number of zero-crossings for  $X_2$ , which is the number of antinodal points, is also tracked during the integration for checking the consistency of the algorithm.

A similar numerical scheme was used by Holman and Bowen (1979) to solve a set of equations which are the equivalents of equations (11a, b) in dimensional form. Those authors used a polynomial to represent the bottom profile and determined the wavenumber by maximizing the offshore distance at which the solution diverges. We found that the process of maximizing the offshore distance is rather ambiguous and results in an inefficient search for the wavenumber. The algorithm described in the previous paragraph

avoids this ambiguity by matching the number of nodes and antinodes with the mode number and uses the measured profile directly in the algorithm without decomposing it into a polynomial.

The algorithm was tested by comparing the numerical results with those obtained from the existing analytical solutions for the linear and the exponential profiles. The comparison showed agreement of the dispersion relation to an accuracy consistent with the value of the error index ( $e_r$ ) used in the algorithm. Furthermore, the numerical results for the exponential profile also give the same cutoff mode number as that given by the analytical solution (equation 10). The model results presented in this paper were obtained using an error index of 0.01% which, for the linear and the exponential profiles, gives wavenumbers to within 0.01% of those predicted by the analytical solutions. Figure 1 shows the model prediction of the amplitude function for a constant slope beach and a pronounced bar-trough beach. The presence of the bar apparently increases the wave amplitude near the bar crest, particularly those of the waves that have an antinode located over the bar crest.

#### FIELD OBSERVATIONS FROM A BAR-TROUGH SURF ZONE

Beach profiles of Eastern Beach, in southeastern Australia, are used as the model profiles. The beach was the location of an 11-day field study from May 5 to May 16, 1981 (Wright et al., 1986). Instrumented pods supporting ducted current meters and pressure transducers were deployed simultaneously at several stations across the surf zone to measure the currents and the wave heights. Bottom profiles were surveyed daily using a conventional theodolite and a surveying level. Between the upper limit of the beach face and the inner edge of the bar, the bottom profiles are

characterized by a near exponential form of  $h=h_0[1-\exp(-\alpha x)]$ . For example, on May 10, the profile during low tide gave  $h_0=1.7\text{m}$  and  $\alpha=0.06$ . A pronounced bar, with water depths less than 1 m during low tides, persisted throughout the experiment and migrated ~40 m shoreward from an initial position of ~100 m seaward of the beach face. Figure 2 shows a series of beach and surf zone profiles. In reality, the surf zone exhibited a degree of three-dimensional rhythmicity (Wright and Short, 1984). This rhythmicity was subtle at the beginning of the experiment, but became more pronounced as the bar migrated shoreward.

Long period swells, originating in the Southern Ocean, dominated the incident wave conditions throughout the field observation period. Typically, incident swell periods were between 12 and 16 seconds (0.063-0.083 Hz). Offshore wave measurements at  $h=20\text{ m}$  and  $h=10\text{ m}$  showed peak periods of ~14 seconds. Incident swell heights were characteristically around 1-1.5 m. Shorter period ( $T=6-8\text{ s}$ ) incident waves superimposed their effect on the background swell during gales. Tide range during the experiment was less than 0.5 m.

Spectra and cross spectra of  $\eta$  and  $u$  from different locations within the trough of Eastern Beach revealed strong standing wave motion across the subharmonic and infragravity frequencies. Figure 3 shows examples of the  $\eta$  and  $u$  spectra from the two stations inside the trough. These data were measured on May 11, 1980 during low tide. As indicated by a phase difference of  $\pm 90^\circ$  between  $\eta$  and  $u$ , frequencies lower than ~0.07 Hz (~16 s) which include a portion of the incident swells, are standing. In a pure standing wave, all energy at nodes is kinetic (maximum velocity amplitude, zero surface elevation) whereas at antinodes all energy is potential. Changes of the phase difference from  $90^\circ$  to  $-90^\circ$  or vice versa

indicate the presence of nodes or antinodes. Two nodes and one antinode, marked by small arrows in the figure, can be identified in each set of spectra.

The numerical model developed in the previous section was used to compute the offshore distances of the nodes and antinodes at various wave periods. Figure 4 shows the distributions of the first and the second nodes and the second antinodes for the low tide beach profile on May 11. For convenience, we designate the first antinode to be at the beach face even though it does not satisfy the conventional definition of antinode (i.e.  $\zeta'=0$ ). The distributions have a band-like structure. The upper curve of each band shows the node or antinode distributions of the leaky mode waves and the lower curve show that of the lowest possible edge wave mode. The positions of the node or the antinode for the higher mode edge waves lie between the two curves. Also shown in Figure 4 are the nodal and the antinodal periods obtained from the  $n-u$  cross spectra of the observed data (e.g. Figure 3). Overall, the observed node and antinode periods agree well with the model predictions.

Of particular interest is the position of the antinode relative to the bar crest. The large slope at the shoreward edge of the bar and the shallow depth over the bar crest favor reflection of the waves propagating seaward from the beach face. Waves with their antinodes located over the bar may be trapped and become more energetic as a result of resonance. On the other hand, waves with their first nodes located over or seaward of the bar may be suppressed because of the flow restrictions produced by the shallow depth over the bar. The selective resonance of waves with antinodes over the bar and the suppression of waves with nodes over the bar was reported by Symonds and Bowen (1984) based on a numerical model study. Our model prediction

(figure 1) shows a greatly enhanced amplitude over the bar crest for a near resonant wave. Because of the length restriction, waves with periods between 62 s and 71 s will have their first node located over the bar. Only those waves with period less than 33 s may have their antinodes (other than the one at the beach face) located over or shoreward of the bar. If our stated hypotheses concerning standing wave resonance and suppression are true, there will be a relatively energetic subharmonic and high frequency infragravity wave band (<33 s) and a weak long period infragravity wave band (>60 s) in a pronounced bar trough surf zone.

To examine the hypothesis of wave resonance and wave suppression, we combine the potential ( $gS_n(f)$ ) and the kinetic ( $h[S_u(f)+S_v(f)]$ ) energy spectra into a single total energy spectrum,

$$S_t(f) = gS_n(f) + h[S_u(f)+S_v(f)] , \quad (12)$$

where  $S_n$ ,  $S_u$  and  $S_v$  are the spectral estimates of  $\eta$ ,  $u$ , and  $v$  respectively. In deriving (12), we use the shallow water wave approximation and consider the oscillatory currents to be uniform throughout the water column. The corresponding total energy density,

$$\bar{E} = \frac{\rho}{2} [h(\overline{u^2} + \overline{v^2}) + \frac{g}{2} \overline{\eta^2}] ,$$

can be reduced to

$$E_* = h_* \zeta_*^2 + (1 + h_* k_*^2) \zeta_*^2, \quad \text{where } E_* = \frac{4\bar{E}}{\rho g a_0^2} \quad (13)$$

Thus, the total energy density distribution is a function of the offshore distance and shows no longshore variation even for the edge wave mode. Figure 5 shows the distribution of  $E_*$  for a 30 s wave whose amplitude function is shown in figure 1. For the leaky wave mode,  $k_* = 0$  and  $E_* = h_* \zeta_*^2 + \zeta_*^2$ . The total energy density for the leaky mode wave decreases gradually with offshore distance except near the bar crest where the presence of the bar produces a slight increase in the energy density.

Spectral troughs and peaks that occur in conventional  $\eta$  or  $u$  spectra as a result of the presence of nodes and antinodes are eliminated in the leaky mode total energy spectrum. Thus, for a known leaky wave motion, the total energy spectra from different locations in the surf zone can be compared. A spectral peak in the total energy spectrum observed at a specific location in the surf zone should occur at the same frequency in the total energy spectrum obtained at a different location.

The distributions of the total energy density of the edge wave modes are more complicated. A redistribution of the total energy density occurs resulting in the total energy density becoming concentrated near the antinode, this is particularly pronounced for the mode 1 edge wave. As the mode number increases, the total energy density distribution of the edge wave rapidly approaches that of the leaky mode wave. Thus, for the higher mode edge wave, spectral peaks in the total energy spectrum will be likely to occur at the same frequencies across the surf zone. At the lower modes (e.g. mode 1 or 2), it is more difficult to determine whether, for a known edge wave motion, spectral peaks in the total energy density will occur at the same frequencies across the surf zone. However, shoreward of the position of the second antinode, the variations in the total energy density distributions are well behaved and differ only slightly for waves of different mode. Since waves with periods greater than  $\sim 14$  s have their second antinodes of the lower mode edge waves located over or seaward of the bar crest, the spectral peaks observed in this range will probably occur at the same frequencies across the trough.

Examples of the total energy spectra for the data collected during a low tide event are shown in Figure 6a. The significance of using the total energy spectrum can be demonstrated by comparing the total energy spectra

with the individual  $\eta$  and  $u$  spectra in Figure 3. While the spectral peaks and troughs for the individual  $\eta$  and  $u$  spectra at the two stations occur at different frequencies, the spectral peaks of the total energy spectra for the two stations occur at the same frequencies. These spectral peaks of the total energy spectra occur within the subharmonic and the higher infragravity frequency bands which fall into the frequency range where one expects the antinodes to lie over the bar. Although the significance levels of some of the peaks are marginal, that they occur consistently at the same frequency at both stations is significant. The spectral trough occurring between 0.01 Hz and 0.02 Hz is consistent with the notion that waves with a node over the bar should be suppressed even though the minor peak in the high tide spectra may indicate a possible forcing by the groupiness of the incident waves. An increase in the spectral density at the very low frequencies ( $<0.01$  Hz) is caused by the strong longshore velocity component associated with the lateral circulation of the bar-trough surf zone. Further evidence of selective amplification of the resonant wave can be found in Figure 7. These data were taken on May 8 when the bar was located further offshore. Again, the spectral peaks of the two spectra occur at the same frequencies. The two major peaks at 17 s and 33 s satisfy the predicted resonant wave periods of the mode 1 and mode 2 edge waves respectively. Again, a spectral trough, occurring between 0.01-0.02 Hz, indicates long wave suppression. The higher energy density at frequencies less than 0.01Hz is again related to the strong longshore velocity component. These results support our hypothesis that there is a selective trapping of wave energy in the trough at the resonant frequencies and a possible suppression of the long infragravity waves in a bar trough surf zone.

## EFFECTS OF TIDAL ELEVATION CHANGES AND BAR MIGRATION

Over a tidal cycle, the water depth in the trough and the distance between the beach face and the bar crest vary. As the tide rises from low to high, the distance between bar crest and the beach face widens. Although this should increase the periods of the waves with node or antinode over the bar, model predictions indicate that the increase is counter-balanced by the increase in water depth which decreases these periods by increasing the propagation speed of the wave. Numerical calculations showed a slight decrease in the resonant wave periods and the wave period for waves satisfying nodes over the bar at high tide (Table 1). This is evident in the observed total energy spectra. Figure 6b shows the total energy spectra at high tide using data collected approximately six hours following the low tide observations shown in Figure 4 and 6a. There is a subtle shift of the spectral peaks toward higher frequencies. The most prominent feature of contrast between the high tide and low tide spectra is the presence at high tide and absence at low tide of the low frequency energy centered around 0.015Hz. Implications are that standing waves in this frequency region which would have nodes over the bar are more effectively suppressed at low tide when the depth over the bar is the least. Figure 8 shows the predicted and the observed positions of the nodes and antinodes for the high tide profile. The predicted range of periods with nodes over the bar is reduced to 58-66 s while the period range for waves with second antinodes over the bar is reduced to 9-30 s which embraces incident swells and their subharmonics (Table 1).

In Figures 4 and 8, the curves showing the antinodal position of the mode 1 edge wave bend sharply upward at a location slightly seaward of the bar crest. This indicates that the second antinode of the mode 1 edge wave

with wave period between 10-25 s is trapped near the bar crest. Within this period range, which covers the long period swells and their possible subharmonic waves, the mode 1 edge wave roughly satisfies the resonant condition. The trapping of the antinodes of edge waves is a feature created by the presence of the bar and was pointed out by Kirby et al. (1981). Unfortunately, our field data were insufficient for confirming the edge wave nature of this energy.

Bar migration alters resonant frequencies. In a bar trough type beach, bar migration is particularly active during high incident wave energy but is also frequent even under moderate or low incident wave conditions (Sallenger et al., 1985; Wright et al., 1986). As the bar migrates, the positions of nodes and antinodes are shifted. Resonant periods increase or decrease depending on the offshore or onshore bar migrations respectively and the longshore edge-wave length changes correspondingly. Figure 9 shows the predicted change in the positions of nodes and antinodes as the bar migrated 20 m offshore. Although the nodal and antinodal positions inside the original trough remained unchanged, their locations shift offshore at regions seaward of the initial bar crest as a result of the increasing water depth. The phenomenon of antinode trapping over bar of the mode one edge wave (for period 10-30 s) persists although with a slight increase in the range of wave period.

During the 11-day experiment, the bar migrated 40 m shoreward from an initial distance of 105 m from the beach face (Figure 2). Numerically predicted resonant periods and the associated longshore wave lengths for the profiles shown in Figure 2 are listed in Table 2. Only the high tide profiles are used in the calculation. The leaky mode wave sets the upper bound of the resonant wave period which decreased from 45 s to 32 s as the

bar migrated 40 m shoreward. A mode 1 edge wave determines the lower bound of the resonant wave period which varies only slightly, from 15 s to 12 s, and is separated from the possible resonant periods of the higher edge wave modes. Because of the antinode trapping of a mode 1 edge wave over the bar, the mode one edge wave with periods ranging from the lower bound to ~25 s roughly satisfies the resonant condition. The predicted longshore wave lengths decreased as the bar migrated shoreward. Thus, shoreward bar-migration would be accompanied by a decrease in resonant period and in longshore edge wave length.

Our investigation on the effects of bar migration has relied on the numerical predictions due to a lack of prolonged field measurements. Although the numerical model predicts that an onshore bar migration results in a reduction in the resonant period and the longshore wave length, which may lead to a reduction in rip spacing and the length scale of the longshore topographic features, it is not clear what mechanism or mechanisms are responsible for initiating the onshore bar migration. Conceivably, a reduction in the incident wave period may set off a reduction in the period of the resonant subharmonic wave and a decrease in the offshore distance of the position of the second antinode. This may favor onshore bar migration.

#### CONCLUSIONS

We examined the characteristics of standing waves on a pronounced bar-trough surf zone by numerically modeling the standing waves over the observed natural topography and comparing the numerical results with field observations.

Field observations showed that waves with periods greater than 16 s were standing in the trough. The nodal and antinodal positions of standing

waves as predicted by the model indicate that for waves with period between 60-70 s, the first node of the standing wave will be located over the bar whereas the nodes of longer periods will be located seaward of the bar. There is evidence that the bar may suppress the waves which have their first node located over bar, as suggested by Symonds and Bowen (1984).

For waves with period less than 45 s, it is possible for the second antinode to be located over the bar or inside the trough. Those with an antinode over the bar satisfy the resonant condition and may result in a selective trapping of wave energy in the trough. Total energy spectra calculated from field data suggest, albeit inconclusively, that a selective trapping of wave energy in the expected resonant frequency band may operate in nature.

Two factors may favor self-maintenance of the pronounced bar-trough beach: (1) the small tidal range that results in a relatively constant resonant condition throughout the tidal cycle, and (2) the resonant condition which results from the trapping of antinodes of the edge wave modes over the bar.

Cross shore migration of the bar changes the resonant condition and the longshore edge wave length. Onshore bar migration is accompanied by a reduction in the longshore wave length of the edge wave mode and may lead to a reduction in the spacing of the rip current and possibly, other macro-scale longshore topographic features of the bar-trough beach.

#### ACKNOWLEDGEMENTS

This study has been supported by the Office of Naval Research, Coastal Sciences Program Task NR 388-189, Contract N00014-83-K-0198. Beach and surf

zone surveys were conducted by A.D. Short and J. Mackaness. We are also grateful to ESSO Australia for funding assistance for the field study. The following individuals provided essential professional assistance with the field study: P. Nielsen, P.J. Cowell, F.C. Coffey, M.O. Green, M.P. Bradshaw, and G. Lloyd.

## REFERENCES

- Ball, F.K., Edge waves in an ocean of finite depth. *Deep Sea Res.*, 14, 79-88, 1967.
- Eckart, C., Surface waves on water of variable depth. Wave Rep. 100, Ref. 51-12. Scripps Inst. of Oceanogr., Univ. of Calif., La Jolla. 99pp, 1951.
- Gerritsen, F. and J. van Heteren, Low frequency oscillations on the Dutch coast. Proc. 19th ICCE, Houston, Texas, p. 625-641, 1985.
- Holman, R.A. and Bowen, A.J., Edge waves on complex beach profile. *J. Geophys. Res.*, 84, 6339-6346, 1979.
- Hull, T.E., Enright, W.H. and Jackson, K.R., User's Guide for DEVRK - A subroutine for solving non-stiff ODE's. TR No. 100, Dept. of Computer Science, Univ. of Toronto, 1976.
- Katoh, K., Multiple longshore bars formed by long period standing waves. Rep. of the Port and Harbour Res. Inst., V. 23, No. 3, 1984.
- Kirby, J.T. Jr., Dalrymple, R.A. and Liu, P.L.F., Modification of edge waves by barred-beach topography. *Coastal Engineering*, 5, 35-49, 1981.
- Sallenger, A.H., Holman, R.A. and Birkemeier, W.A., Storm-induced response of a nearshore-bar system. *Mar. Geol.*, 64, 1985 (in press).
- Symonds, G. and Bowen, A.J., Interactions of nearshore bars with incoming wave groups. *J. Geophys. Res.*, 89, 1953-1959, 1984.
- Wright, L.D., Field observations of long-period surf zone standing waves in relation to contrasting beach morphologies. *Aus. J. Mar. Freshwater Res.*, 33, 181-201, 1982.
- Wright, L.D. and Short, A.D., Morphodynamic variability of surf zones and beaches: A synthesis. *Mar. Geol.*, 56, 93-118, 1984.

Wright, L.D., Nielsen, P., Shi, N.C. and List, J.H., Morphodynamics of a  
bar-trough surf zone. Mar. Geol., 1986 (in press).

Table 1. Range of wave period with node or antinode over bar.

	1st node over bar		2nd antinode over bar	
	Mode 1	Leaky mode	Mode 1	Leaky mode
	Edge wave		Edge wave	
Low tide	62 s	71 s	11 s	33 s
High tide	58 s	66 s	9 s	30 s

Table 2. Resonant wave periods (T) and corresponding longshore wave lengths (L) for the beach profiles shown in Figure 2. The center of the flat portion of the bar is used as the bar position for estimating equilibrium antinodal location.

Profile	Mode 1		Mode 2		Mode 3		Leaky mode	x(bar)
Date	T(s)	L(m)	T(s)	L(m)	T(s)	L(m)	T(s)	
May 5	15	72	40	405	41	530	45	105m
May 7	15	70	40	387	41	510	43	100m
May 8	13	60	34	260	35	366	32	83m
May 10	12	60	30	220	31	290	33	77m
May 16	12	55	27	180	30	267	32	65m

## FIGURE CAPTIONS

- Figure 1. Amplitude function  $\zeta(x)$  for a constant slope beach and a pronounce bar trough beach (wave period = 30 s). Shown in the figure are the leaky (L) mode and up to mode 3 edge wave solutions.
- Figure 2. Changes of the beach profile during the experiment.
- Figure 3. Spectra of  $\eta$  and  $u$  at stations B and C during low tide on May 11, 1981. The station locations are shown in Figure 4.
- Figure 4. Predicted positions of nodes and antinodes for the low tide profile. Field observations are represented by the dots and the circles.
- Figure 5. Cross-shore variation of the total energy density distribution calculated based on the low tide profile shown in Figure 4 (wave period = 30 s).
- Figure 6. Total energy spectra of the low and high tide data at stations B (dash line) and C (solid line) on May 11.
- Figure 7. Total energy spectra at stations B (dash line) and C (solid line) on May 8.
- Figure 8. Predicted positions of nodes and antinodes for the high tide profile. Field observations are represented by the dots and the triangles.
- Figure 9. Predicted changes in the positions of nodes and antinodes due to bar migration.

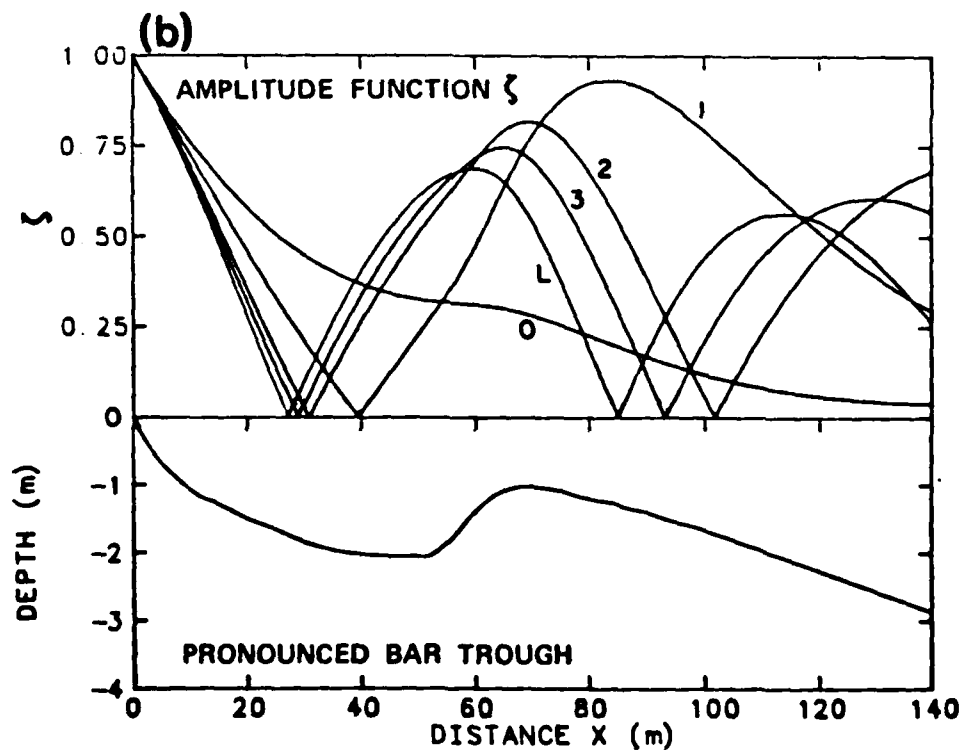
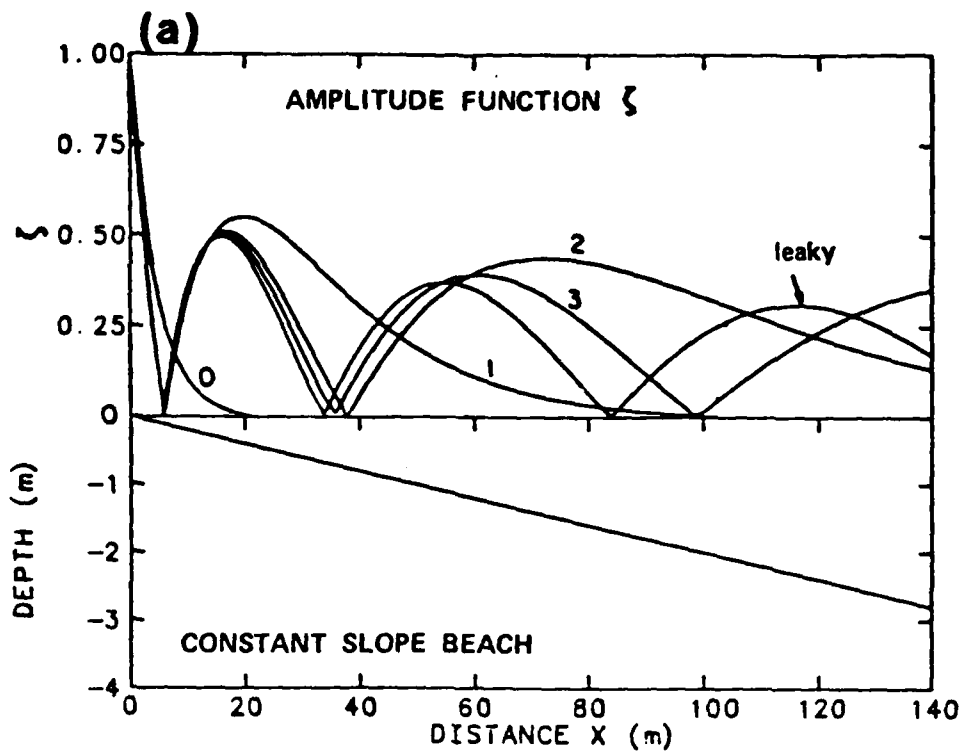


Figure 1. Amplitude function  $\zeta(x)$  for a constant slope beach and a pronounced bar trough beach (wave period = 30 s). Shown in the figure are the leaky (L) mode and up to mode 3 edge wave solutions.

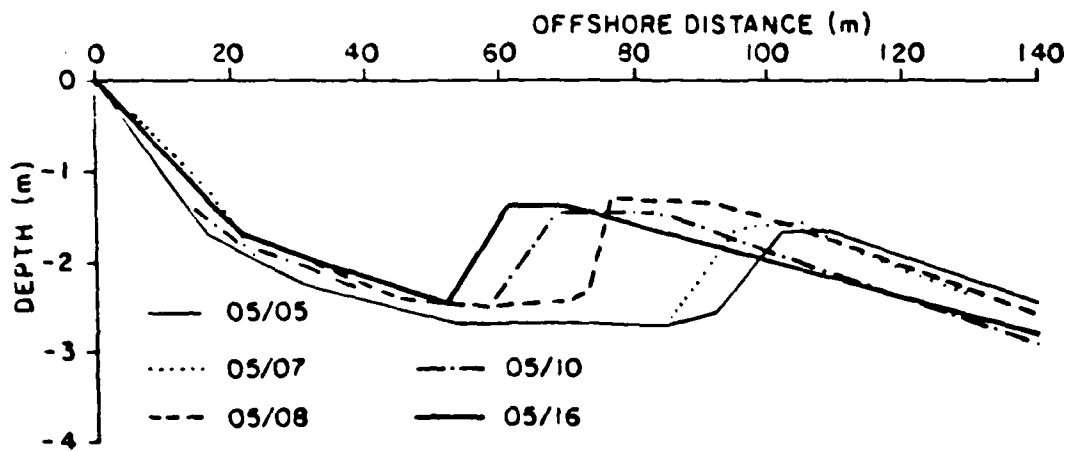


Figure 2. Changes of the beach profile during the experiment.

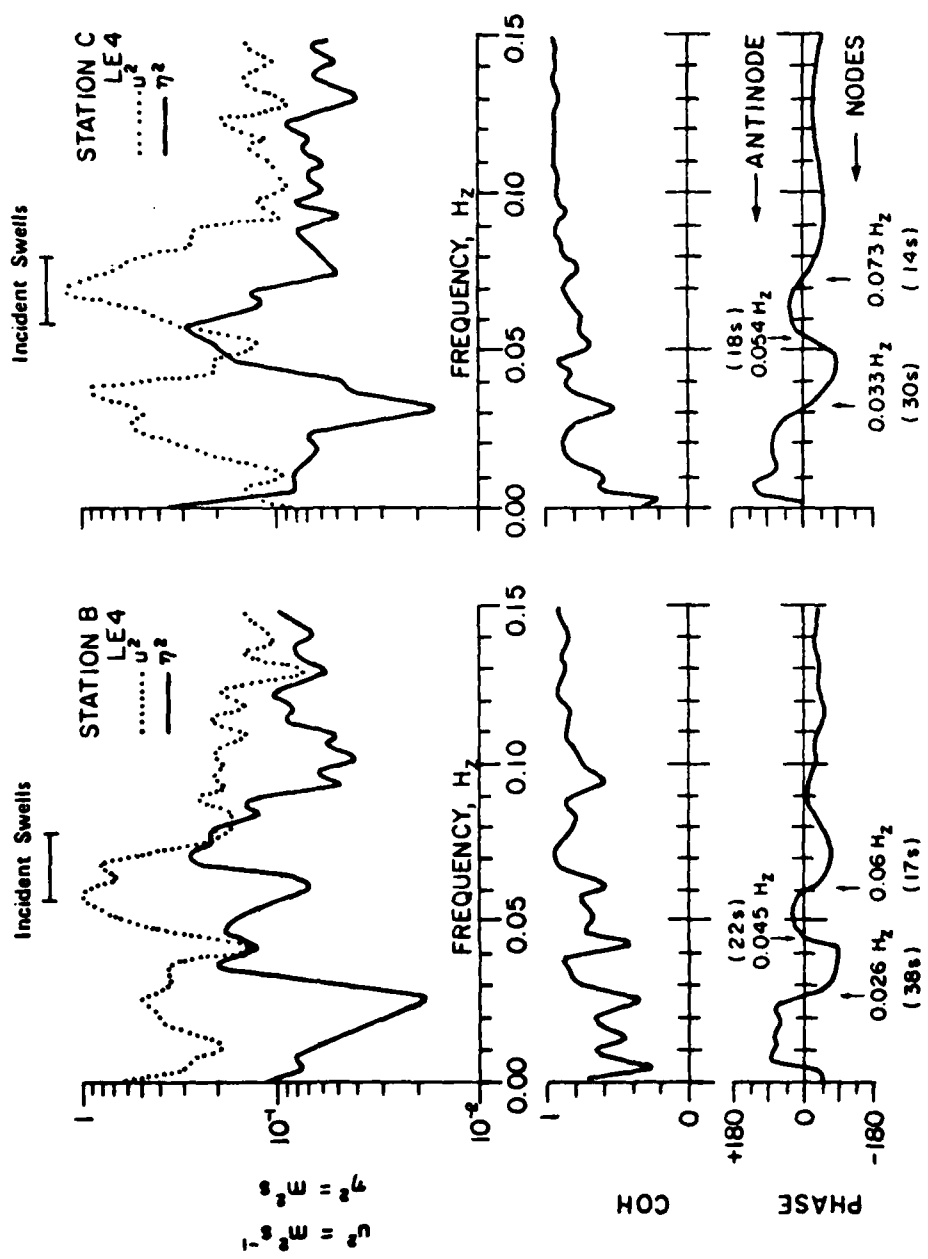


Figure 3. Spectra of  $\eta$  and  $u$  at stations B and C during low tide on May 11, 1981. The station locations are shown in Figure 4.

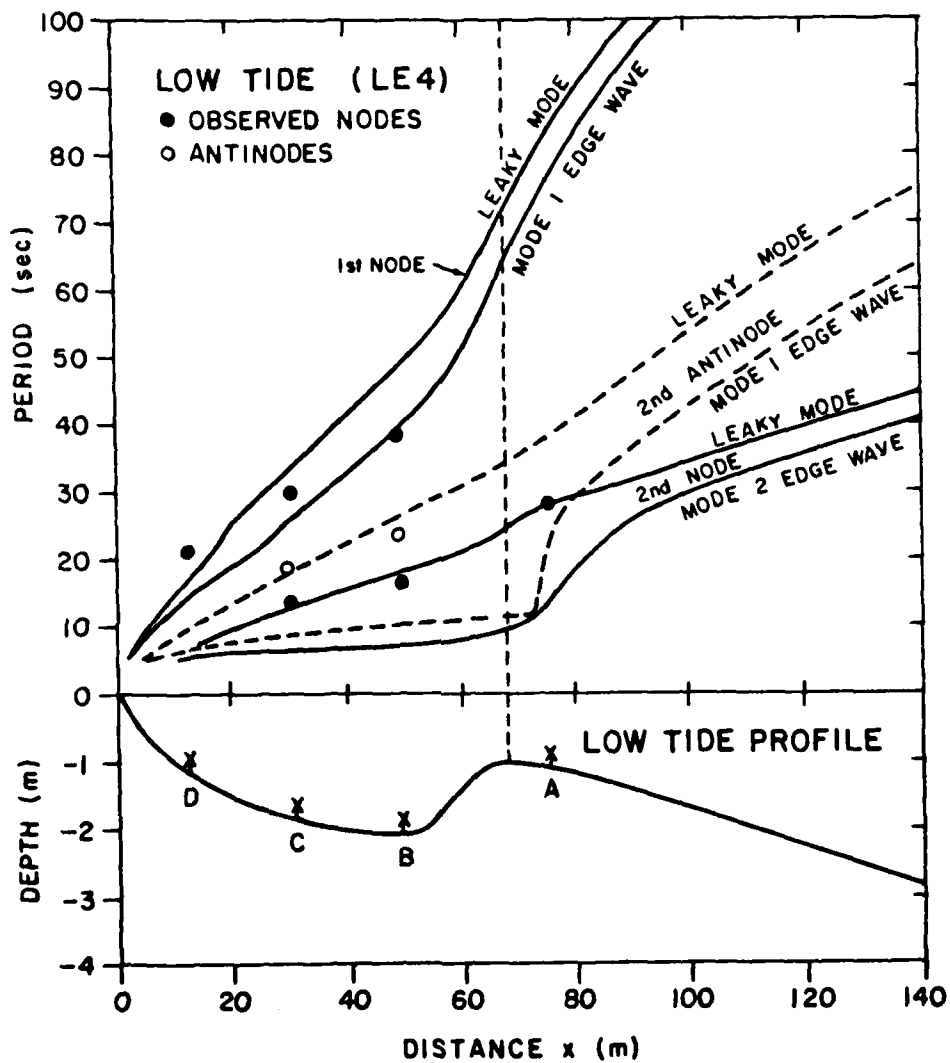


Figure 4. Predicted positions of nodes and antinodes for the low tide profile. Field observations are represented by the dots and the circles.

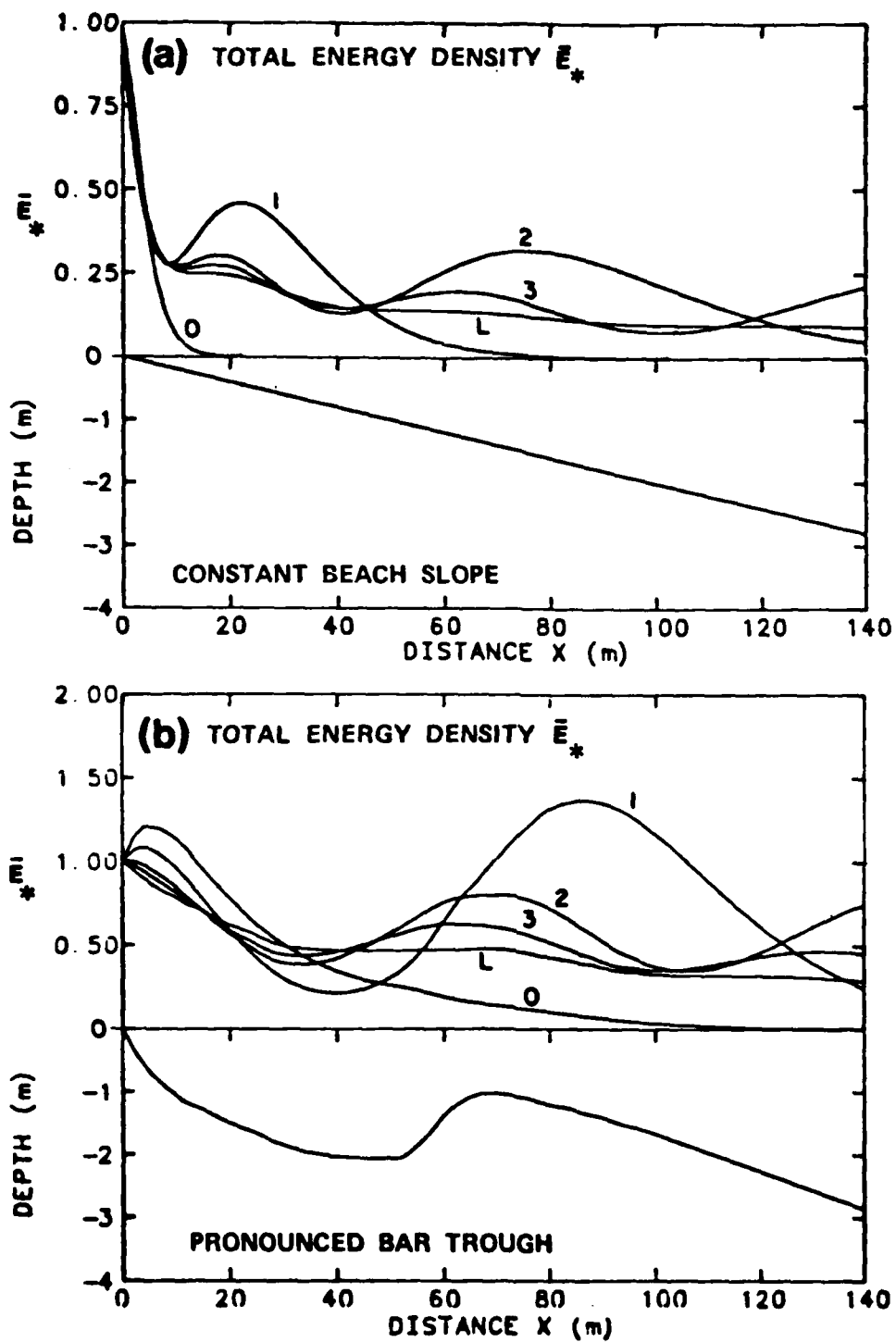


Figure 5. Cross-shore variation of the total energy density distribution calculated based on the low tide profile shown in Figure 4 (wave period = 30 s).

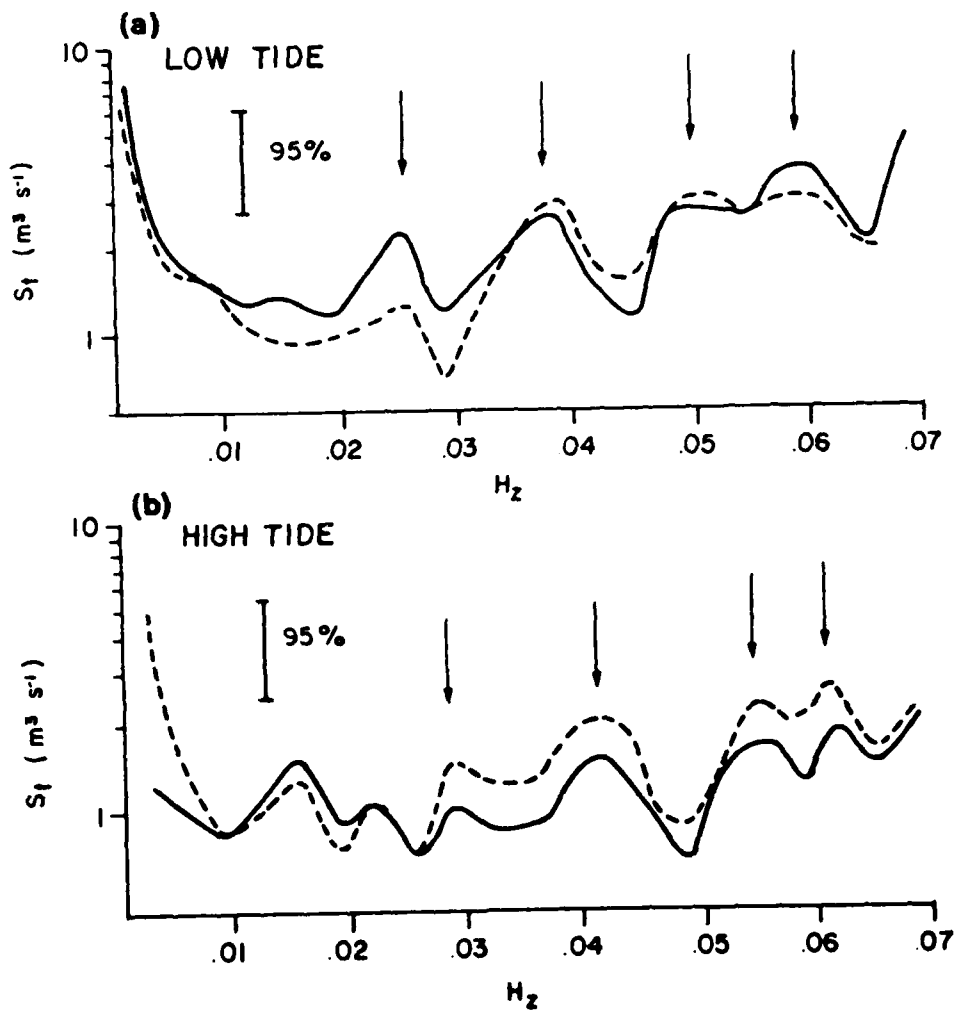


Figure 6. Total energy spectra of the low and high tide data at stations B (dash line) and C (solid line) on May 11.

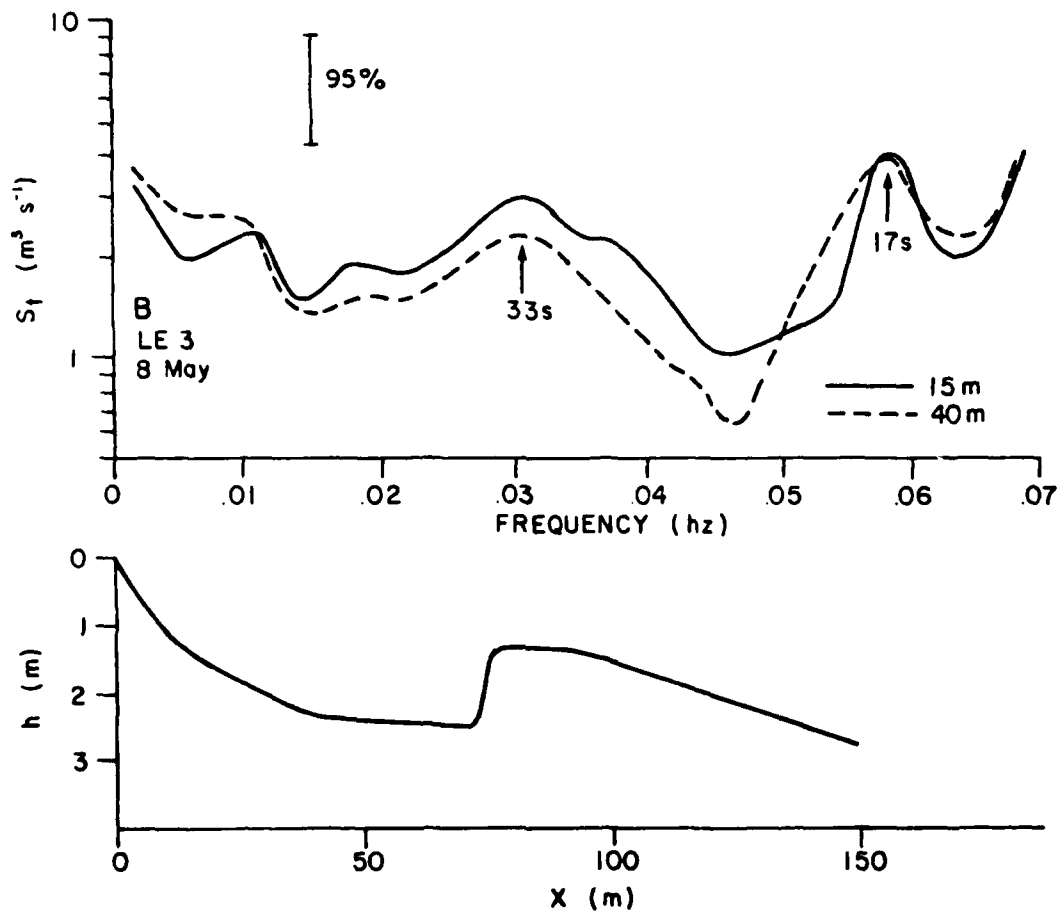


Figure 7. Total energy spectra at stations B (dash line) and C (solid line) on May 8.

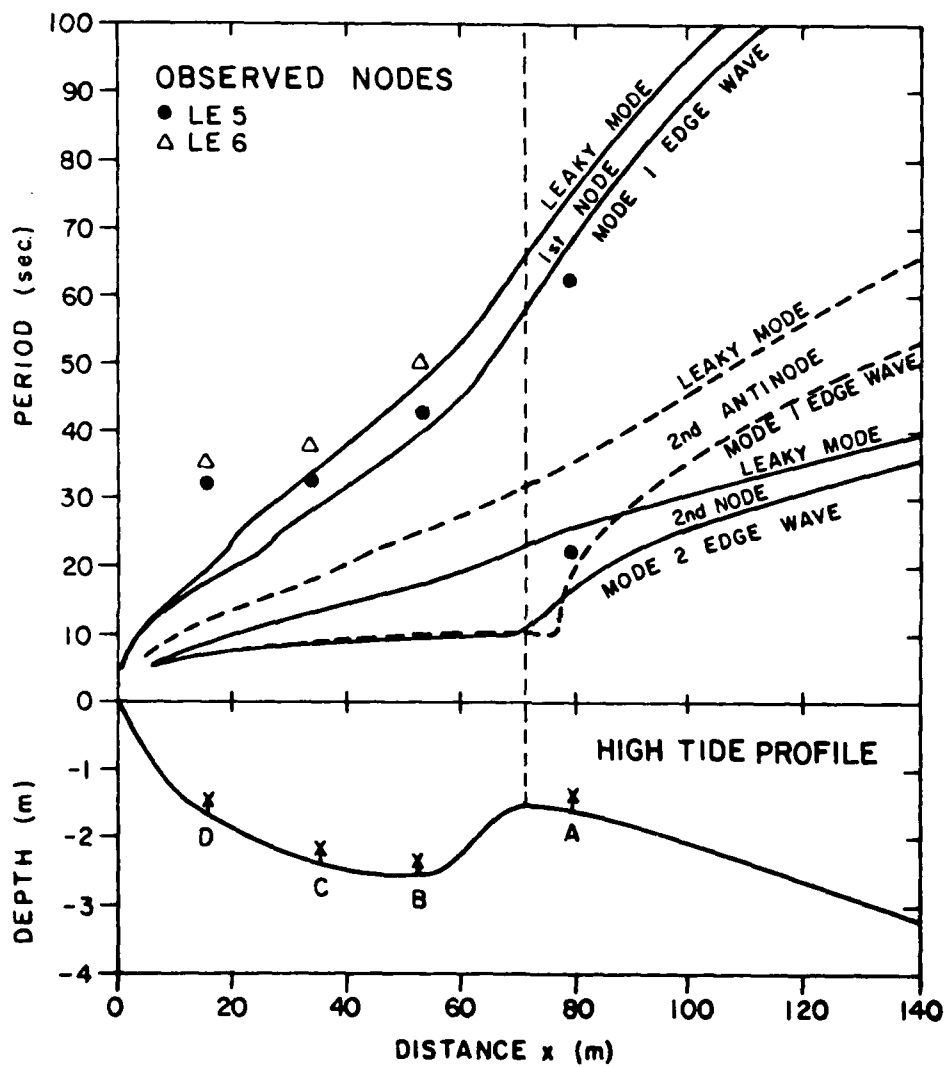


Figure 8. Predicted positions of nodes and antinodes for the high tide profile. Field observations are represented by the dots and the triangles.

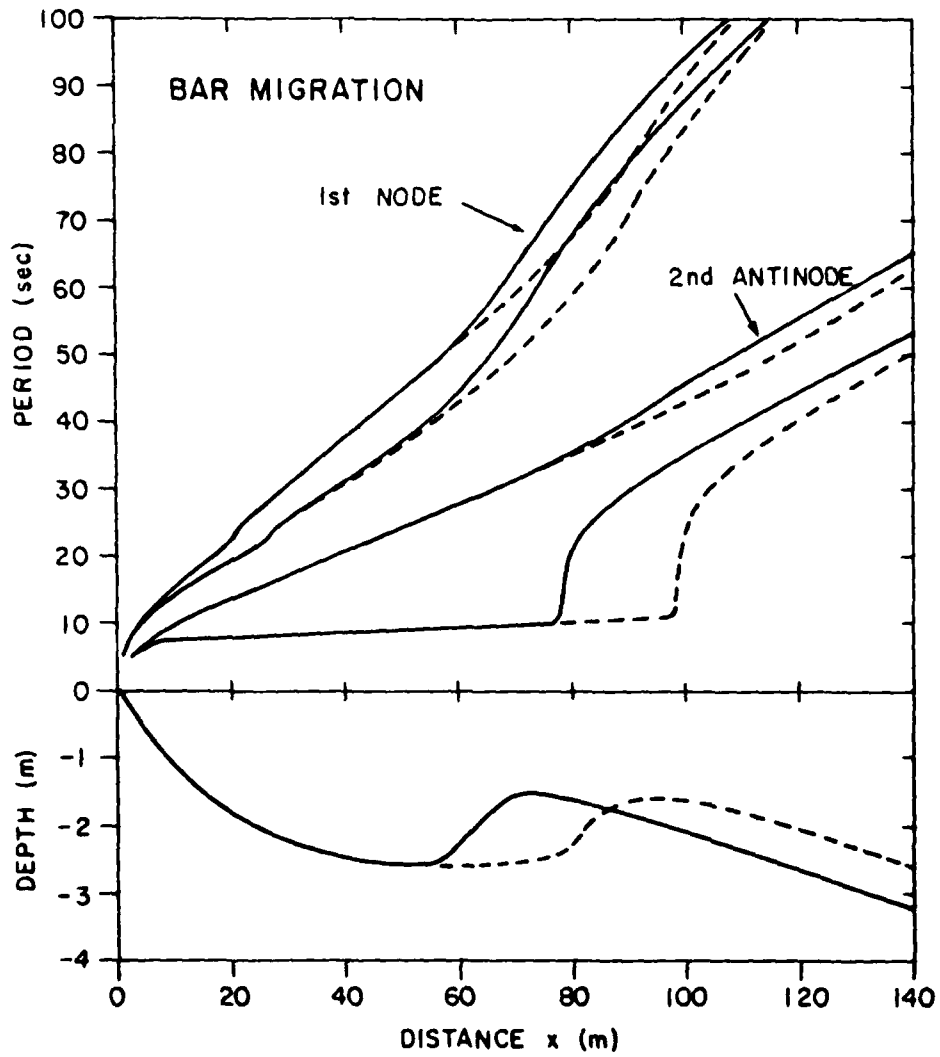


Figure 9. Predicted changes in the positions of nodes and antinodes due to bar migration.

**END**

**FILMED**

*2-86*

**DTIC**